

## Chapter 04

# Magnetoencephalography (MEG) as a Technique for Imaging Brain Function and Dysfunction

Likan Zhan\*

Institute for Speech Pathology and the Brain Science, Beijing Language and Culture University, China

**\*Corresponding Author:** Likan Zhan, Institute for Speech Pathology and the Brain Science, Beijing Language and Culture University, Beijing 100083, China, Email: zhanlikan@hotmail.com

First Published **August 24, 2018**

This Book Chapter is an excerpt from an article published by Likan Zhan at "Experimental Linguistics"(English translation). (Likan Zhan. Introduction to Magnetoencephalography. *Experimental Linguistics*. 2018; 7(1):7-11)

Copyright: © 2018 Likan Zhan.

*This article is distributed under the terms of the Creative Commons Attribution 4.0 International License (<http://creativecommons.org/licenses/by/4.0/>), which permits unrestricted use, distribution, and reproduction in any medium, provided you give appropriate credit to the original author(s) and the source.*

## Abstract

Magnetoencephalography (MEG) [1,2] is a neural imaging technique (-Graphy) using an array of sensitive magnetic flux sensors positioned over the scalp to measure the biomagnetic (Magneto-) inductions produced by bioelectric activity in the brain (Encephalo-). Although different sensing technologies are maturing [3,4], the present industry standards normally rely on cryogenically cooled superconducting sensors, i.e., Superconducting Quantum Interference Devices (SQUIDS). Henceforth, this article will briefly explain the properties of these cryogenic based MEG systems and their applications in the neuroscience: the basic property biomagnetic signal; the basic principles of MEG; the basic components of a state-of-art MEG system; the commercial MEG systems in the market; the comparison between MEG system and other neuroimaging systems; the potential clinical and diagnostic applications of the MEG system.

## Bioelectromagnetism

### Electrophysiological Basis of MEG Signals

In the nervous system, neural cells are basic units of information processing. A neuron consists of a *cell body*, several *dendrites* that receive input from other neurons, and a single *axon* that sends information out. A neuron is immersed in the intracellular fluid and is separated from the extracellular space by a membrane. The membrane has selective permeability to different ions, resulting in a  $70mV$  electric charge inside the neuron.

Applying a stimulus to the synapse changes the neuron's membrane permeability and generate a *synaptic potential* between  $70mV$  and  $55mV$ . The neuron is conductive, so the synaptic potential will cause a current flowing within the cell, called *primary current* or *impressed current*, and a return current outside of the cell, called *volume current*. A synaptic potential current travels slowly from the dendrites to the axon, and lasts up to tens of milliseconds. The magnitude of a postsynaptic potential varies with the strength of the stimulus. Its

magnitude can also be summated if a stimulus is applied repeatedly in rapid succession, or if stimuli from different sources occur close together. If a postsynaptic potential reaching the axon hillock exceeds  $55mV$  an *action potential* will be generated. An action potential current propagates fast along the axon without decreasing in strength, and lasts only about 1 millisecond. This swiftness makes the temporal summation of action currents less effective than that of synaptic currents.

A primary postsynaptic potential currents can be adequately described by a single current dipole oriented along the dendrite (Figure 1a), while the primary action potential current should be approximated by a pair of opposite current dipoles (Figure 1b). This makes the magnetic fields generated from a postsynaptic potential falls off more slowly with distance (in proportion to  $1/r^2$ ) than the field associated with the quadrupolar action potentials (in proportion to  $1/r^3$ ) [5-7]. These two differences make the electromagnetic signals observed outside of the head are largely due to synaptic potentials, rather than action potentials. In special cases, action potentials might also contribute to high-frequency (about 600Hz) electromagnetic fields outside of the skull.

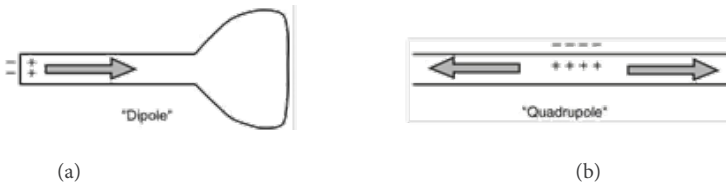


**Figure 1:** Postsynaptic potential and action potential [5].

Human brain contains multiple layers, and the outermost layers of the brain, the cerebral cortex, are the main sources of MEG signals. The total surface area of the cerebral cortex is about  $2.5 \times 10^5 \text{ mm}^2$  [8], with at least  $2.5 \times 10^{10}$  neurons and  $2.4 \times 10^{14}$  synapses in total [9]. There exist approximately  $10^5$  neurons and  $10^9$  synapses per  $\text{mm}^2$  of cortex. Furthermore, one postsynaptic potential generates a  $20 \times 10^{-15}$  ampere current dipole moment. A  $20 \times 10^{-9}$  ampere dipole moment is

required to generate a measurable magnetic field outside of the head, corresponding to about  $10^6$  synapses simultaneously active. Theoretically, the simultaneous activation of as few as 0.1% synapses over an area of  $1 \text{ mm}^2$  would suffice to produce a detectable signal. But the recorded currents are largely concealed when neighboring neurons are fired misalignedly or when different currents are opposite to each other. Up to 93% of the synaptic activity can be shadowed by the spatiotemporal misalignment and asynchronies. In practice, an about  $25 \text{ mm}^2$  area of active cortex would correspond to a  $20 \times 10^{-9}$  dipole moment, i.e. a measurable signal [5,6].

Currents with opposite directions will conceal each other, so only *open fields* can generate a measurable signal out of the head (Figure 2). Each *pyramidal neuron* in the cortex has thousands of apical dendrites that are oriented parallel to each other, so *pyramidal neurons* are the principal type of neurons that generate open fields. Pyramidal neurons are perpendicular to the cortical surface, so the longitudinal intracellular currents flowing along dendrites or axons are also perpendicular to surface of the cortex. According to *Ampère's circuital law*, a magnetic field perpendicular to the current dipole will also be generated.

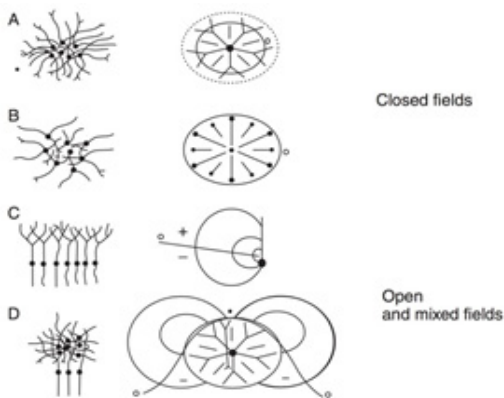
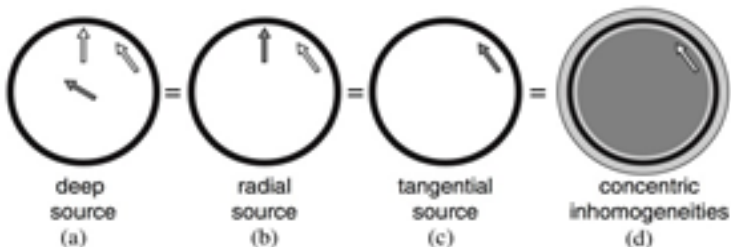


Figure 2: Closed and open fields [10].

## Magnetoencephalography and Electroencephalography

The bioelectromagnetic signals are generated inside the brain, while the cortex MEG sensors to record the magnetic fields are placed outside of the brain. To infer the current sources from the recorded surface signals, a model of the head is needed. *Sphere model* is the simplest one, where the head is approximated with a layered spherically symmetric conductor. Given this model, the magnetic field of a dipole can be derived from a simple analytic expression, where the magnetic field is determined by the center of symmetry, but is irrelevant to the conductivities or thickness of the layers.

In a spherically symmetric conductor, radial currents (Figure 3, b) do not produce any magnetic field outside the conductor. Any current in the center of the sphere is essentially a radial current (Figure 3, a). Given this sphere model, only the tangential currents that are not deep in the center of the sphere will produce magnetic fields outside the spherical surface (Figure 3, c-d).



**Figure 3:** Current dipoles and Magnetic fields [5].

Because pyramidal neurons and corresponding currents dipoles are perpendicular to the cortical surface, so the cortical surface has to be parallel to the surface of the skull, to generate an observable magnetic field. The cortex of human brain are folded in the skull to form gyri and sulci: Neurons at the top of a gyrus have apical dendrites that are perpendicular to the overlying skull, while neurons on

the wall of a sulcus are parallel to the skull (Figure 4). So observable magnetic fields are mainly from a sulcus rather than a gyrus.

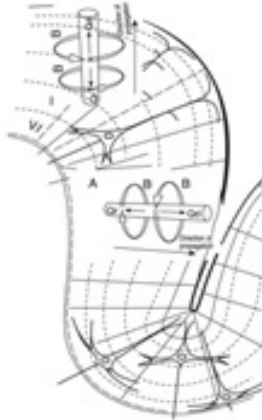


**Figure 4:** Gyrus and Sulcus [10].

*Electroencephalography* (EEG) records the electrical activity generated by the current dipole by placing the electrodes along participants' scalp (Figure 5). The current an EEG records is the volume current that leaks out of the scalp, not the primary current per se, because the primary current are generated in the brain. On the contrary, MEG is most sensitive to the fields generated from the primary currents, as the magnetic field components generated by volume currents in a spherical conductor tend to conceal each other. Magnetic fields are less distorted than electric fields by the heterogeneity of conductivity within head tissues, such as insulating skull and conducting scalp. So MEG needs a simpler model than EEG to localize the source of the signal, with a better spatial resolution. Further-more, MEG is reference-free, while scalp EEG relies on a reference which makes interpretation of the EEG data difficult.

EEG also has some advantages compared to MEG. First, the decay of electric fields as a function of distance is less pronounced than that of magnetic fields. Therefore, EEG is more sensitive than MEG

for deeper sources. Furthermore, EEG is sensitive to both tangential and radial components of a current source in a spherical volume conductor, while MEG is sensitive only to tangential components.

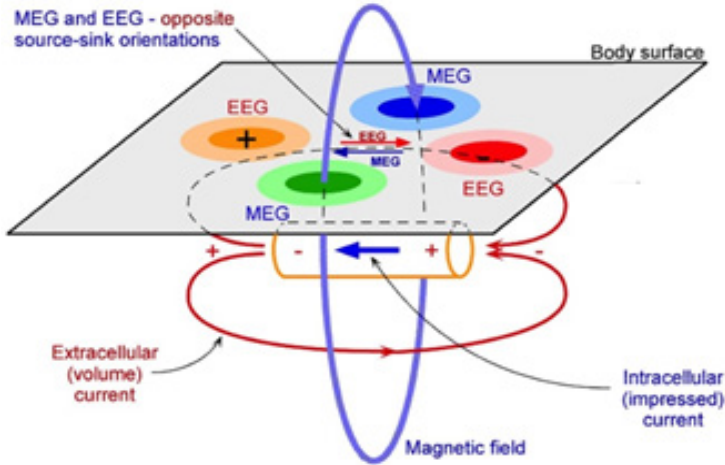


Figure 5: EEG and MEG [11].

## MEG Fundamentals

### Superconductors

MEG measurements of brain activity are currently made using an array of super-conducting sensors placed around the head<sup>1,4</sup>. These cryogenically cooled sensors have femtotesla (fT) sensitivity, which is needed to detect the weak magnetic fields produced by the brain. Unfortunately, the requirement for cooling means that sensors must be housed within a liquid helium dewar with a vacuum space separating sensors from the scalp.

*Superconductors* (Figure 6) are materials that will lose electrical resistance completely when cooled down to a sufficiently low temperature, *critical temperature* ( $T_c$ ). Niobium ( $T_c = 9.2K$ ), mercury ( $T_c =$

4.2K, Heike Kamerlingh Onnes, Nobel Prize in Physics in 1913), and lead ( $T_c = 7.2\text{K}$ ) are typical superconductors used in MEG. Coolants are needed to keep material under the critical temperature. The most commonly employed coolant in MEG is Liquid helium (LHe), whose boiling point is 4.2 kelvins.

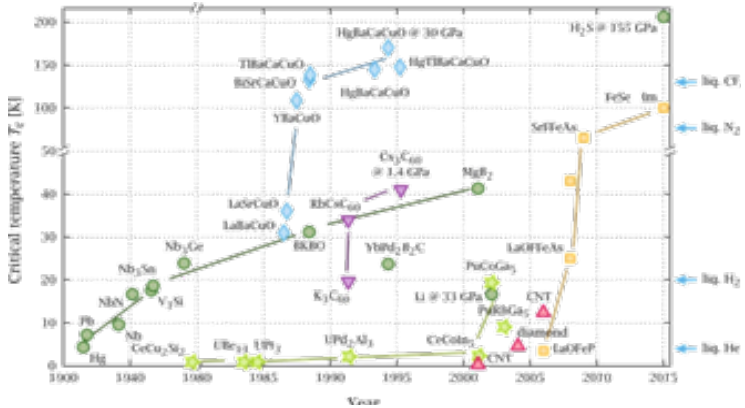


**Figure 6:** Timeline of Superconductivity. (<https://en.wikipedia.org/wiki/Superconductivity>)

## Flux Quantization

A property of superconductors is when forms a superconducting loop, the magnetic flux threading the ring has to be an integral number of the *flux quantum*,  $n\Phi_0$ , where  $n \neq 0$ ;  $\Phi_0 = 2.07 \times 10^{-15}$  Weber. BCS theory [12], (Noble Prize in Physics in 1972) is the only theory so far to successfully explain the superconductivity in low temperature. According to BCS theory, a normal conductor has resistance because the movements of electrons in the conductor are deflected by impurities, defects, and lattice vibrations. Deep cooling will quiet the lattice vibrations and make two electrons of opposite spin and momentum bind together to form a *Cooper pair*. A Cooper pair has a zero net spin and momentum, so it can propagate through the material with-

out resistance, resulting in *superconducting*. According to BCS theory, a *wave function* can be used to describe the probability for a given particle to be in a particular place at a particular time. A single wave function can describe the entire collection of Cooper pairs in a superconductor. When the superconductor forms a superconducting loop, the single wave function around the superconducting ring has to be continuous (Figure 7). This continuity of the wave function requires that the magnetic flux threading the ring has to be an integral number of the *flux quantum*.



**Figure 7:** Flux quantization.

(<http://www.supraconductivite.fr/en/#applications-squid-quantification>)

When a superconductor is placed in a magnetic field, a screen current  $\Phi/L$  will be induced, where  $\Phi$  is the applied magnetic flux and  $L$  is the inductance of the superconductor. If the superconductor forms a ring, the final screen current around the ring will be summated from two currents with opposite directions: the current on the outer surface of the ring and the current on the inner surface of the ring. The current on the outer surface of the ring is determined by the applied magnetic flux, while the current on the inner surface of the loop is determined by the magnetic flux threading the superconducting ring.

On one hand, if the applied magnetic flux is in the contour of  $[n \Phi_0, (n+1/2) \Phi_0)$ , the flux quanta threading the ring will be  $n \Phi_0$ , generating a current  $n \Phi_0/L$  on the inner surface of the ring. The final screen current around the ring will be between  $[0; 1/2 \Phi_0)/L$ . To be

specific, if the applied magnetic flux is  $n \Phi_0$ , the final screen current will be 0. On the other hand, if the magnetic flux is in the contour of  $[(n + 1/2) \Phi_0, (n + 1) \Phi_0]$ , the flux quanta threading the ring will flip to  $(n + 1) \Phi_0$ , generating a current  $(n + 1) \Phi_0/L$  on the inner surface of the ring. The final screen current will be between  $[(1/2) \Phi_0/L; 0]$ . To be specific, if the applied magnetic flux is  $(n + 1/2) \Phi_0$ , the screen current will be  $(1/2) \Phi_0/L$ .

To summarize, the screen current around the ring varies between  $[1/2 \Phi_0/L; 1/2 \Phi_0/L]$ , depending on the applied magnetic flux.  $\Phi$  So the final screen current provides an indirect measure of the applied magnetic field. Nevertheless, the current cannot be readily measured as the conventional current measurement will destroy the continuous superconducting loop and the flux quantization will disappear.

## Josephson Junction

A *Josephson junction* is a superconductor separated by a thin layer of insulating material (Figure 8). When the insulator is thin enough, a super-current can tunnel through the junction without resistance, making Josephson junction a *weak superconductor*. If a circulating current is smaller than the maximum super-current ( $I_c$ ) on the Josephson junction, no terminal voltage will be induced. If the circulating current exceeds its critical current, the Josephson junction will revert to normal state and a terminal voltage will be induced. The critical current of a specific Josephson junction depends on the size of the junction, the superconducting material and the temperature.

This effect is named after Brian David Josephson who theoretically predicted this effect and was awarded a Nobel prize in Physics in 1973 [13]: When two superconductors are separated by a layer of insulating material, the wave functions of the two superconductors will overlap if the insulator is thin enough. If the overlap is sufficiently large, Cooper pairs will be able to tunnel through the barrier without breaking up.

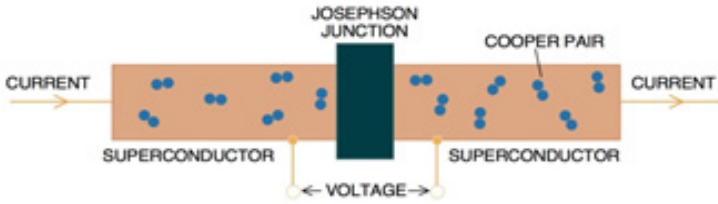


Figure 8: Josephson Junction [14].

## Superconducting Quantum Interference Device

A Superconducting Quantum Interference Device (SQUID) is a superconducting ring interrupted by one (Figure 9, a) or two (Figure 9, b) Josephson junctions. Dc SQUIDs have lower noise levels, much simpler electronics, and minimal crosstalk between channels, so dc SQUID are nowadays preferred in commercial MEG systems. We will use dc SQUIDs to explain how a SQUID works.

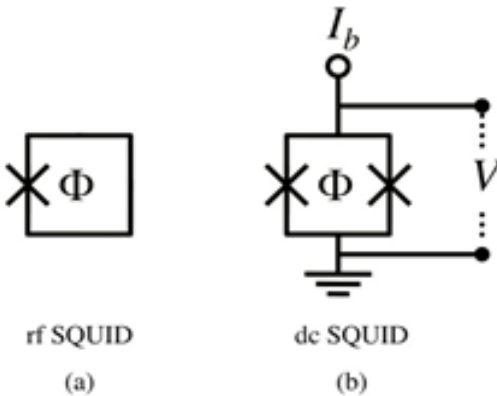


Figure 9: Superconducting Quantum Interference Device (SQUID).

A current-biased dc SQUID is a flux-to-voltage transducer. In the current-biased configuration, a dc SQUID is first biased by a direct current. The terminal voltage between the two ends of the SQUID are then recorded to infer the applied magnetic flux. In a dc SQUID, the bias current equally splits into the two Josephson junctions. One half has the same direction as the screen current, and the other half has the opposite direction to the screen current.

The final circulating current tunnelling a Josephson junction will be the sum-mation of the screen current  $I_s$  and half of the bias current  $I_b/2$ . If the circulating current exceeds its critical current  $I_c$  on either of the Josephson junction, a terminal voltage  $V$  will be induced. The smallest bias current needed to elicit a terminal voltage depends on the applied magnetic flux:  $I_b \geq 2(I_c - I_s)$ . If the applied magnetic flux is  $n \Phi_0$ , no screen current will be induced,  $I_s = 0$ , and the biggest bias current is needed to induce a terminal voltage,  $I_b \geq 2I_c$  (Figure 10, a, red line). If the applied magnetic flux is  $(n + 1/2) \Phi_0$ , the biggest screen current  $\Phi_0/2L$  will be induced, and the smallest bias current is needed to generate a terminal voltage,  $I_b \geq 2I_c - \Phi_0/L$  (Figure 10, a, blue line).

If the bias current  $I_b (\geq 2I_c)$  is kept constant (Figure 10, a, dotted vertical line), changes in the applied magnetic flux will cause the terminal voltage  $V$  swing between two extrema, producing a voltage oscillation with period of  $\Phi_0$  (Figure 10, b, green line).

## Flux-lock loop

The terminal voltage has a nonlinear and periodic relation to the applied magnetic flux, and changes in the magnetic field larger than half of a flux quantum will lead to ambiguous results, so the recorded terminal voltage on the SQUID cannot be directly used to infer the applied magnetic flux. *Flux-lock loop* is a standard method to linearize voltage-flux relation and to read out the SQUID signal. The loop artificially generates an additional magnetic flux to the SQUID loop, conceals the changes of the actual flux to be measured, and locks the output of the SQUID to a certain operating point.

When the SQUID is subject to an artificially generated sinusoidal magnetic flux, with a peak-to-peak-amplitude  $\Phi_0/2$  and a frequency  $fm$ , an ac terminal voltage with two spectral components  $fm$  and  $2fm$  will be induced. The amplitude of terminal voltage differs depending on different static magnetic fluxes. If the static magnetic flux is  $n \Phi_0$  (Figure 11, a), the terminal voltage is a rectified sine wave with the frequency  $2fm$ . If the static magnetic flux is  $(n + 1/4)\Phi_0$  (Figure 11, b), the terminal voltage becomes a sine wave with the frequency  $fm$ . As one increases the static magnetic flux from  $n\Phi_0$  to  $(n + 1/4)\Phi_0$ , the terminal voltage at the frequency  $fm$  steadily increases. In contrast, if instead we decrease the static magnetic flux from  $n \Phi_0$  to  $(n - 1/4) \Phi_0$ , the voltage at the frequency  $fm$  steadily increases in a negative direction (Figure 11, c) [15,16].

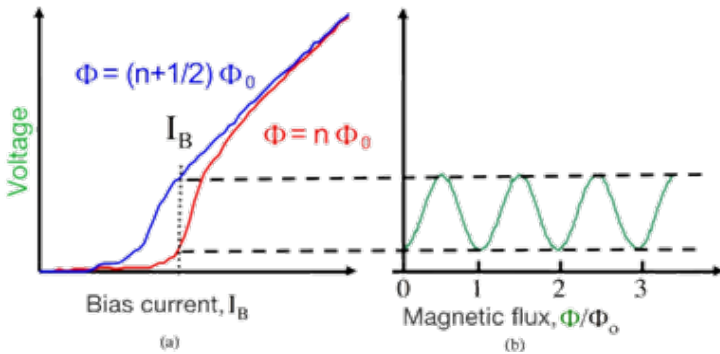


Figure 10: Bias current, voltage, and magnetic flux.

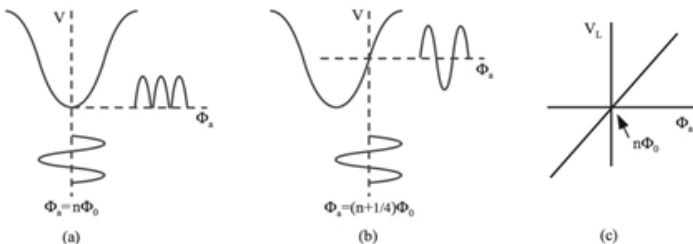


Figure 11: Flux Modulation [17].

The alternating voltage across the SQUID is coupled to a low-noise preamplifier, usually at room temperature. After amplification, the signal from the SQUID is lock-in detected and sent through an integrating circuit. By referencing to the same oscillator generating the sinusoidal modulation flux, the lock-in detector will be gated at the frequency  $f_m$ , and the output will be similar to figure 11, (c). After integration, the resulting signal is fed back as a current through a resistor to a coil, thus keeping the flux in the SQUID constant at an optimum working point. If the applied magnetic flux induces a magnetic flux deviation from the working point, an opposing flux will be applied to cancel the deviation. The output voltage  $V_f$  across the feedback resistor  $R_f$  will be proportional to the derivation. The MEG signal recorded is not the SQUID output itself, but the inverted negative feedback signal. This feedback signal has a linear relation with the measured signal, even if the changes is larger than a flux quantum.

In conjunction with suitable feedback electronics locking the measured flux to maintain a stable operating point, a SQUID can reach a resolution of  $10^{-6}\Phi_0$  Wb. However, the frequency and intensity a SQUID can measure are limited by the electronics that is used. An analog electronics operating at room temperature offers a frequency range from dc to kHz, with a dynamic range (the ratio of the maximum to the minimum signal amplitude) of 120 dB or more. A broadband digital electronics can offer a frequency up to low MHz, with a dynamic range up to near 200dB [18].

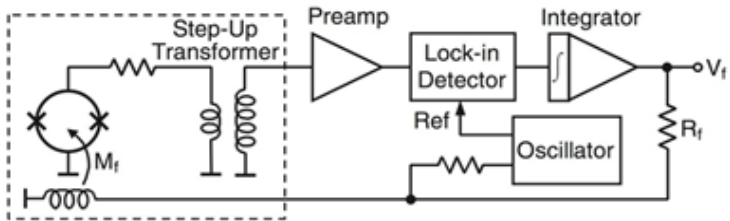


Figure 12: Flux-lock loop [19].

## Practical MEG Systems

### SQUID Fabrications

The real SQUID body is normally fabricated as a square washer with a small hole in the center and two slits to the outer edge (Figure 13a): The relative large outer dimension (  $75\text{ }\mu\text{m}$  ) enhances the loop's sensitivity, while the relative small inner dimension (  $25\text{ }\mu\text{m}$  ) reduces its inductance and noise level [20]. And the Josephson junctions (*JJ*'s) on slit at the bottom edge of the washer are about  $5\text{--}7\text{ nm}$  thick [21]. The superconductors, tunnel barrier, insulator, and the resistors around the Josephson Junction of a low-temperature transition SQUID are normally made of *Nb*, *Al-AIO<sub>x</sub>*, *SiO<sub>2</sub>*, and *Al* respectively.

To further increasing the loop's efficient area without boosting its inductance, a *flux transformer* is normally coupled to the SQUID washer. A flux transformer is a closed superconducting circuit consisting of a *pick-up coil*, a pair of interconnecting leads, and an *input coil* coupling to the SQUID washer. A magnetic field applied to the pickup coil induces a super-current in the transformer and a flux in the SQUID. A pick-up coil is much larger than the SQUID, making it more sensitive than bare SQUID washer. Figure 13b shows a simplified version of a multi-turn spiral input coil integrated on the top of the washer to couple the captured signal. One more coil is used to couple the feed back signal from the flux-lock loop (Figure 13, c).

### Flux Transformers

Different pick-up configurations have been fabricated in literature. The simplest configuration is a *magnetometer* (Figure 14a), which consists of a single superconducting coil loop and no compensation coil. The pick-up loop is much larger than the SQUID, making it sensitive to the biomagnetic signals, as well as ambient magnetic noises.

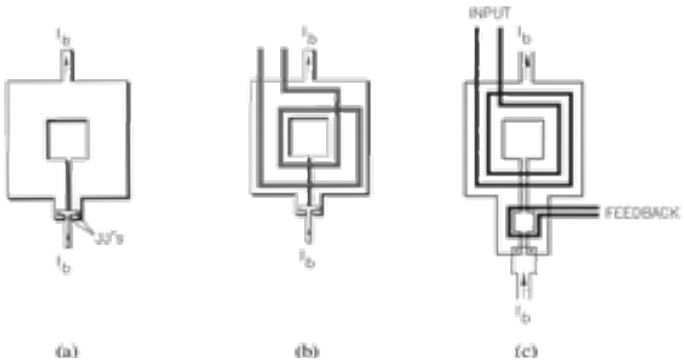


**Figure 13:** A practical SQUID [22].

One or more compensation coils are normally added to decrease the flux transformers' sensitivity to the ambient magnetic noise. This configuration is called *spatial gradiometers*, which measures the spatial gradient of a magnetic field component, rather than the magnetic field component itself. The basic logic behind this configuration is that far away magnetic sources generate homogeneous magnetic fields near the flux transformer. When the pick-up coil and the spatially nearby compensation coil are wound in opposite directions, no net shielding current will be produced by the far-away magnetic sources. This configuration makes the spatial gradiometer blind to sources distant enough to be seen as homogeneous fields. And a spatial gradiometer is able to detect the weak signals against a background of magnetic noise many orders of magnitude higher. The number and the spatial allocation of the compensation coils differ between different sensor types.

An *axial gradiometer* measures the change of the radial field component along the radius, by placing the coils along the same radial axis, with the pickup coil being several centimeters closer (*baseline*) to the head than the compensation coil. A larger baseline makes the sensor more sensitive to the deeper sources within the head, with the

tradeoff rejecting less ambient magnetic noises. In a typical *first-order axial gradiometer* (Figure 14b), the pick up coil and the compensation coil are identical in area, connected in series, and wound in opposition, with a baseline of 5 cm. A *first-order planar gradiometer* (Figure 14c) places the coils side-by-side in the same plane.

Both axial and planar gradiometers are insensitive to homogeneous magnetic fields. But their spatial sensitivity patterns or *lead fields* are quite different: the signal from an axial gradiometer peaks for sources around the rim of the sensor while planar gradiometers give the maximum signal for sources right beneath them (Figure 14, bottom row).

### Magnetically Shielded Room

SQUIDS are most sensitive magnetic fields sensors known. With a flux transformer, a SQUID can reach 1ft resolution [14]. This extraordinary sensitivity makes SQUIDS the only feasible device so far to record the weak magnetic fields generated from the brain, which are on the order of 10-100ft.

The brain signals are normally amid much stronger ambient noises and the biomagnetic noises (Figure 15). Sources of ambient magnetic noises include earth's steady field ( $10^{11}$ ft, which is billions of bigger than the brain signal), moving magnetic objects (subways, cars, trucks, elevators etc), electric devices (Television, radio, wifi hotpot, power-line) etc. Sources of biomagnetic noises are from other part of the human body, such as muscles, lung, heart, eyeblinks, etc.

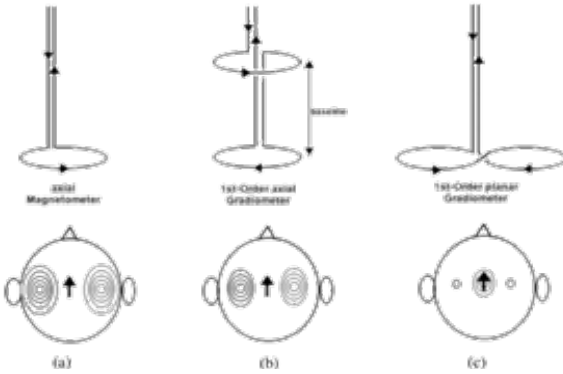


Figure 14: Flux Transformers [7].

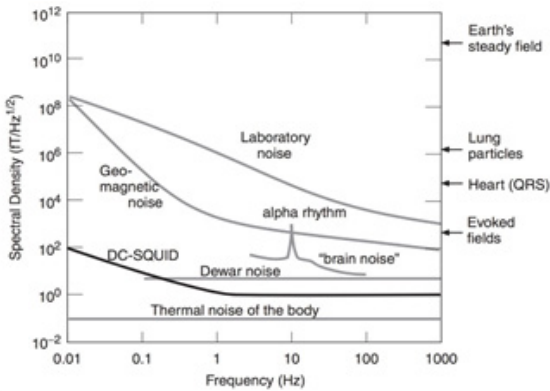
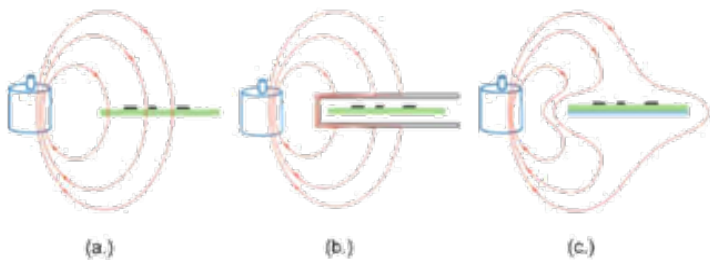


Figure 15: Magnetic field strengths [23].

To successfully measure the MEG signal, the magnetic noises have to be eliminated or attenuated. Spatial gradiometers discussed earlier and reference sensor array are normally used to filter out the unwanted magnetic fields. To keep the strength of the ambient magnetic noises below that of the MEG signal, the now-a-days MEG system is normally installed inside a *magnetically shielded room* (MSR).

The simplest shielding to reduce the magnetic noise inside the room is accomplished by eddy currents using a thick layer of high-conductivity metal (Figure 16c, eddy-current shielding) like Aluminium. Eddy current shielding is effective at 1 Hz and above, but not effective at low frequencies. So high-permeability metal (Figure 16b, ferromagnetic shielding), such as mu-metal (an alloy mostly of nickel and iron) are also used to provide low-frequency attenuation. To increase the *shielding factor*, the ratio the external field to the residual field inside the shielding room, practical MSRs normally employ multiple such layers. An interference field at the location of the MEG system can also be measured and actively concealed by generating a compensating field.



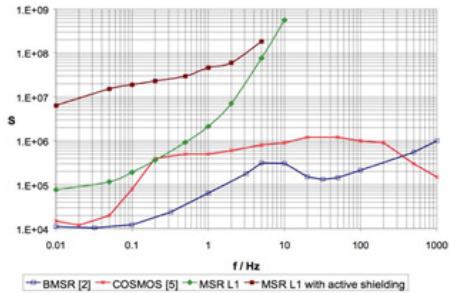
**Figure 16:** Magnetic field shielding (<http://learnemc.com/practical-em-shielding>).

The most commonly used magnetically shielded rooms by far are the ones designed by the Physikalisch Technische Bundesanstalt in Berlin, Germany, and made by VACUUMSCHMELZE GmbH & Co. KG at Hanau, Germany [24]. The wall of their rooms comprises of 7 magnetic layers of MUMETALL with varying thickness and one highly conductive eddy current layer consisting of 10 mm Aluminium. The shielding factor of the chamber is more than  $2 \times 10^{-8}$  above 5Hz, and is  $7.5 \times 10^{-4}$  at 0.01Hz. With the help of active shielding, the shielding factor can achieve over  $2 \times 10^{-6}$  at 0.01Hz.

The shielding room installed in Beijing Language and Culture University is also from this company, with a dimension of  $3508\text{mm} \times 4518\text{mm} \times 2865\text{mm}$  (*width*  $\times$  *depth*  $\times$  *height*), and with a weight of



(a)



(b)

Figure 17: Commercial MSR [24].

## Dewar, Cryogenics, and Gantry

To successfully record the weak MEG signal, a high temperature difference (about 300 K or °C) should be maintained across a small distance: the head surface at body temperature should be close enough ( $\leq 20\text{mm}$ ) to the MEG sensors remaining below the critical temperature. The special equipment *Dewar* is used to fulfill this object. A *Dewar* composes two concentric vessels with a vacuum jacket, where the vacuum prevents heat conducting from the outside to the inside vessel. Helmet-shaped dewars covering the whole head are normally used in modern MEG systems. The dewar is made of fiberglass reinforced plastic, which is non-magnetic and mechanically strong with low thermal expansion coefficient. Multiple layers of superinsulation and thermal shields are also inserted between the inner and outer vessels, to block thermal radiation and reduce the system noises.

Despite the extreme thermal isolation, small heat still leaks into the inner vessel, causing the liquid helium to slowly evaporate. An exhaust line is installed to guide the evaporated gaseous helium out

of the MEG Dewar and the magnetically shielded room. The helium gas is released into the open air outside of the building, or is collected into pressurized containers for reliquification. A typical whole-head system normally reserves 70-90 liters' liquid helium in the MEG Dewar, with a boiling rate of 10-20 liters per day. So 1-3 times of liquid helium refilling are required to keep the system operational. Gaseous helium from a storage tank is used to push the liquid helium from the storage Dewar into the MEG Dewar along a vacuum-isolated siphon. Up to 10 liters of liquid helium evaporates when cooling the siphon from room temperature down to 4.2 K. So at least 10 liters of liquid per transfer should be budgeted for such losses. Recently, practical onsite helium recycling solutions have emerged and approach 90% efficacy, which reduces weekly refills to one or two per year and makes cutting edge MEG technology less expensive and more accessible for researchers.

The *gantry* is the mechanical system supporting the MEG Dewar. It allows adjusting the elevation and angle of the Dewar to accommodate subjects of different heights and in different positions, such as seated or supine. The height adjustment can also be achieved by moving the seat up or down. For safety and accuracy reasons, the gantry should be very rigid, since even minute movements of the sensors in the remanent field inside the shielded room gives rise to artifacts [23].

## Commercial MEG Systems

### ET, Elekta, and CTF

Three main commercial MEG system on the market are Elekta MEG made in Finland [26], CTF MEG made in Canada [27], and ET MEG made in Japan [28]. These systems are different in various facets (Table 1).

First, the dewars are different between these systems. The dewars orientation of Elekta (Figure 18, a-b) and CTF (Figure 18, c-d) systems are adjustable between the vertical and horizontal positions,

which allows both fully supine and seated testing modes. But the the dewar of ET system is gantry-free and horizontal fixed, which allows only supine testing mode (Figure 18, e). Except for its inflexibility, horizontal dewar also has some advantages: the dewar is lower in height and needs a smaller room to install the system. All other neural imaging methods such as MRI are recorded in supine mode, and the brain slightly changes its shape about 3 mm at seated and supine mode. The supine mode makes the comparison between different imaging techniques more reasonable. Furthermore, ETcompany fabricated the horizontal dewar as a ship-in-a-bottle (Figure 18, f). This design largely reduces the boiling off rate of the dewar, by making the bottle neck of the dewar much smaller than the size of the censor complex.

**Table 1:** Comparison between MEG systems.

	Elekta	CTF	ET
Measuring mode	supine/seated	supine/seated	supine
System height	2.3 m	more than 2 m	1.55 m
LHe refilling	1 per week	1 per week	1 per week
Sensor size	28 mm	15 mm	15 mm
Measuring sites	102	275	64-230
Baseline	17 mm	50 mm	50 mm
Censor types	three types	single	single
Sensor noise	5 fHz <sup>1/2</sup>	5 fHz <sup>1/2</sup>	5 fHz <sup>1/2</sup>
	5 fHz <sup>1/2</sup> cm <sup>1</sup>	1 fHz <sup>1/2</sup> cm <sup>1</sup>	1 fHz <sup>1/2</sup> cm <sup>1</sup>

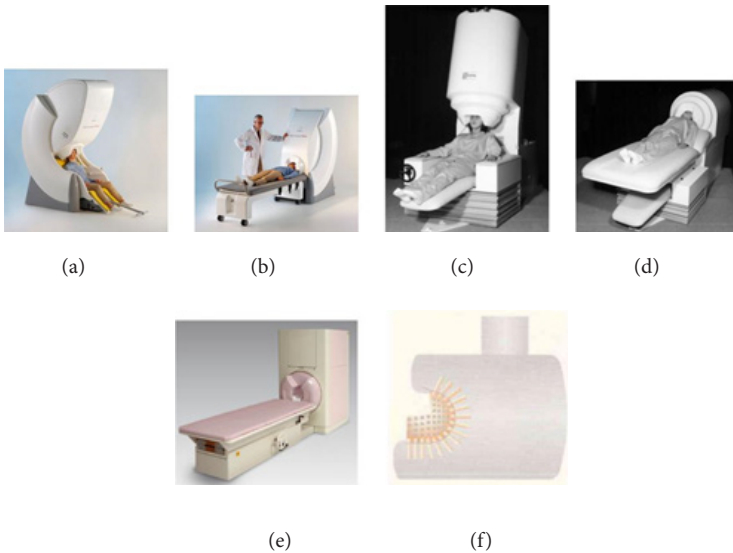


**Figure 18:** Different MEG systems.

Second, the pick-up coils are different between these system. The size of the pick-up coils is 28 mm in Elakta system (Figure 19, a) and is 15 mm in CTF and ET systems (Figure 19, d). Because the surface size of the helmet in the dewar is fixed, bigger size of the pick-up coils means fewer independent measuring sites that are possibly installed. Henceforth, the Elakta system has the smallest number of independent measuring sites: only 102. And CTF system has the biggest number, which is up to 275 sites. The number of measuring sites in ET system is between 64-230. On merit of the CT system is that it allows the expansion of measuring sites after it is installed.

Third, these systems also use different flux transformers. In Elakta system, one magnetometer and two orthogonal first-order planar gradiometers are fabricated in the same measuring site (Figure 19, a), resulting in 306 sensing channels in total (Figure 19, c). The baseline

tween two measuring sites is 17 mm. In CTF and ET systems, one first-order axial gradiometer is fabricated in one measuring site, with the baseline between the measuring coil and the compensating coil is 50 mm (Figure 19, d-e). In spite of these differences, the noise level of the sensors are quite similar among these systems.

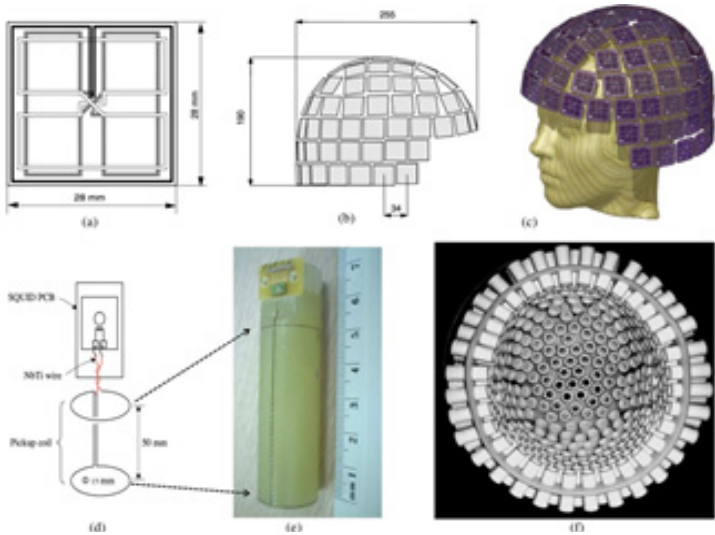


Figure 19: MEG sensors.

## Child, Baby, and Fetal MEG Systems

Magnetic field produced by neuronal currents is inversely proportional to the square of the distance. To efficiently record the weak brain signal, participants' head surface should be close enough to the MEG sensors. Babies and children have smaller heads adults, and the layout of the MEG helmet is fixed. The distance between the sensors and the magnetic sources will be too large to provide an optimal signal-to-noise ratio, when an adult MEG system is used with young children participants. Different special MEG systems have been built to efficiently test children at different ages.

First, ET technology built a child MEG system to test the kids above 3 years' old [29]. The sensor array of the child MEG system is 200m in diameter and is 20% smaller than the conventional MEG sensor arrays (Figure 20). This custom sized helmet can fit about 90% of 7 years' typically developing kids. The child MEG system has been installed in Macquarie university Australia, Tokyo University, Japan, and Beijing Language and Culture University, China, and has been proven useful in increasing the Signal-to-noise ratio in children [30].

Second, Tristan Technologies has build three systems to record the MEG sig-nals from new born babies to kids of 3 years' old. The sensors of these systems are installed in the vacuum between the two vessels, rather than in the inner vessel of the Dewar. This makes the coil-to-surface distance much shorter than conventional MEG systems, and makes the systems sensitive enough to detect the weaker signals generated from young infants and new born babies. The product *babySQUID* (Figure 21a) is designed to assess brain functions in newborns and infants. The system is housed in a moveable cart small enough to be transported from one room to another. To assess brain functions, one places the baby on the bed of the cart and the head on its headrest with MEG sensors just below [31]. The whole-head MEG systems *Artemis123* (Figure 21b) is designed to test kids from 6 months' old to 36 months old [32]. The *MAGView* (Figure 21c) has similar technical specifications as *Artemis123*, but with more channel sensors, 200-400. The sensor of *MAGView* can be configured as gradiometer or magnetometer. The subjects are measured in a supine position, and the helmet can be positioned at a height between 30 to 36 degrees.

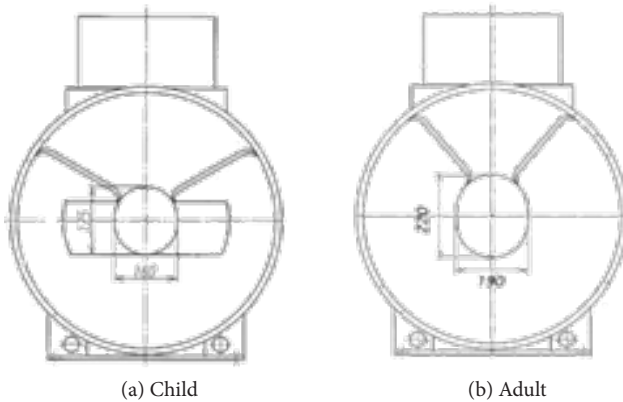


Figure 20: Products of Eagle Technology [29].

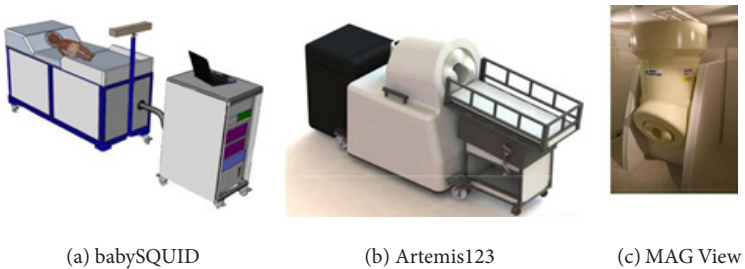


Figure 21: Products of Tristan Technologies.

Third, CTF developed a fetal MEG system to measure the brain activity of unborn fetuses [33]. The fMEG system is operated under the same shielding conditions as the standard MEG systems. An adjustable padded seat matches the height of the perineal dewar extension, so that the mother can sit upon and lean against the sensor surface (Figure 22, a). And the sensor array is shaped to cover the mother's anterior abdominal surface, from the perineum to the top of the uterus (Figure 22, b-c).

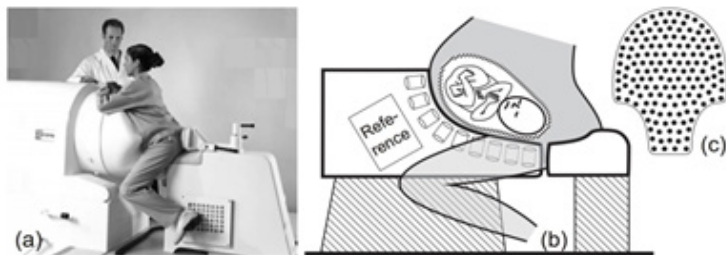


Figure 22: CTF Fetal MEG [34].

The detailed technical specifications of these MEG systems are summarized in table 2.

Table 2: Fetal, newborn, baby, and child MEG systems.

	CTF (fetal)	babySQUID	Artemis123	ET (child)
Age area	before born	new born	0.5-3 yrs	After 3yrs
Shape	pregnant abdomen	headrest	helmet	helmet
Circumference	NA	NA	50 cm	53.4 cm
Coverage area	1300 cm <sup>2</sup>	300 cm <sup>2</sup>	606 cm <sup>2</sup>	whole head
Measuring sites	151	76	123	64-151
References	29	6	12	varies
Censor types	1st axial	1st axial	1st axial	1st axial
Diameter	20 mm	6 mm	15 mm	15 mm
Baseline	80 mm	30 mm	60 mm	50 mm
Sensitivity	5 fT/Hz <sup>1/2</sup>	20 fT/Hz <sup>1/2</sup>	10 fT/Hz <sup>1/2</sup>	5 fT/Hz <sup>1/2</sup>
Coil position	inner vessel	vacuum section	vacuum section	inner vessel
Coil-to-surface	Unknown	6 1 mm	7 1 mm	20 mm

## Comparing with Other Neuroimaging Techniques

First, MEG and EEG are only two of the many neuroimaging methods that are used to measure the brain function. Other neuroimaging methods include: Positron Emission Tomography (PET), Single-Photon Emission Computed Tomography (SPECT), Functional Magnetic Resonance Imaging (fMRI), and Functional Near-infrared spectroscopy (fNIRS).

MEG and EEG directly record the bio-electric-magnetic signals generated in the brain, with a high temporal resolution. The bio-electric signals but not the biomagnetic signals are distorted by the skull and scalp of the head, the EEG will have a poor spatial resolution than a scalp MEG, when the sensors are placed on the surface of the scalp. Under some medical situations, the EEG sensors will be placed under the skull and directly on the surface of the brain, the spatial resolution of the so called electroencephalography (iEEG) or Electrocorticography (ECoG) will be largely improved.

Neurons require oxygen to appropriately function. When a brain area is more active it consumes more oxygen and to meet this increased demand blood flow increases to the active area. The oxygen in blood vessels is distributed around the blood in the form of oxygenated hemoglobin. So the flow of the blood in the circulatory system and the level of oxygenated hemoglobin in the blood are the indirect marker of the underlying neural processes. PET and SPECT inject substance with radioactive isotopes into the blood flow, and measure the local variations in cerebral blood flow by observing the radioactive decay of these unstable isotopes. The proportion of Oxyhaemoglobin and Deoxyhaemoglobin in blood (BOLD) is an index of the local oxygen level. fMRI measures the magnetic fluctuations produced by the BOLD change. It works by detecting the changes in blood oxygenation and flow that occur in response to neural activity –when a brain area is more active it consumes more oxygen and to meet this increased demand blood flow increases to the active area. fNIRS is

an optical technique for measuring blood oxygenation in the brain. It works by shining light in the near infrared part of the spectrum (700-900 nm) through the skull and detecting how much the re-emerging light is attenuated. How much the light is attenuated depends on blood oxygenation and thus fNIRS can provide an indirect measure of brain activity.

**Table 3:** Neuroimaging methods. (adopted from Johnsrude & Hauk, [35]; Min, Marzelli, & Yoo, [36]; Nicolas-Alonso & Gomez-Gil, [37]).]

	Activity	Temporal	Spatial	Risk	Portability
	measured	resolution	resolution		
EEG	Electrical	0.05 s	10 mm	Non-invasive	Portable
ECoG	Electrical	0.003 s	1 mm	Invasive	Portable
MEG	Magnetic	0.05 s	5 mm	Non-invasive	Non-Portable
fMRI	Metabolic	1 s	1 mm	Non-Invasive	Non-Portable
fNIRS	Metabolic	1 s	5 mm	Non-Invasive	Portable
PET	Metabolic	10 s minutes	5-20 mm	Invasive	Non-Portable
SPECT	Metabolic	minutes	20 mm	Invasive	Non-Portable

Second, one advantage of fMRI compared to bioelectromagnetic recording is that the fMRI signal itself is informative enough to localize the source of the signal, while the M/EEG signal itself is insufficient to determine the distribution of electrical currents in the brain. Some priori constraints have to be hypothesized to resolve the inverse problem of M/EEG data. For example, the anatomical information measured from structural MRI can be used to reduce the permissible MEG source locations within the cranial volume or the cortical gray matter. Eagle technology also introduces a five-sensors' marker coil to calibrate and align the relative position between the head of the participant and the sensor arrays [28].

Third, other neuroimaging techniques to explore the structure of the brain include Diffusion Tensor Imaging (DTI), Computed Tomography (CT), and to stimulate the brain function include Transcranial current stimulation (tCS) and Transcranial magnetic stimulation (TMS), where a low current is delivered to certain brain area via electrodes on the scalp (tCS), or via a magnetic field generator (TMS) above the region of the brain.

## Contributions to Neuroscience

The MEG technique has been used to publish about 750 indexed journal articles and conference proceeding entries each year, contributing 5% of all the neuro-science research [38]. These research cover many research areas, including audition [39], vision [40,41], sensorimotor [42], attention [43,44], consciousness [45], speech and language [46-48], and music [50], etc. In the clinical area, the MEG technique has been utilized to presurgically evaluate the epilepsy [51-54], to explore the prospective biomarker of the autism spectrum disorders [55,56], and to study the physiological mechanism the movement disorders [57], etc.

To summarize, among the techniques available to explore and resolve brain function and dysfunction, MEG has the best combination of direct and noninvasive access to the electrophysiological activity of the entire brain. The MEG technique has submillisecond temporal resolution and has ability to resolve activity between cerebral regions with often surprising spatial and spectral differentiation and minimum bias (For more information, please see Baillet, [37]; Hämäläinen & Hari, [5]; Hämäläinen et al., [6]; Hansen, Kringelbach, & Salmelin, [58]; Hari & Salmelin, [59]; Singh, [6]; Supek & Aine, [60]; Vrba, [61]).

## References

1. Cohen D. Magnetoencephalography: Evidence of magnetic fields produced by alpha-rhythm currents. *Science*. 1968; 161: 784–786.
2. Cohen D. Magnetoencephalography: Detection of the brain's electrical activity with a superconducting magnetometer. *Science*. 1972; 175: 664– 666.
3. Boto E, Holmes N, Leggett J, Roberts G, Shah V, et al. Moving magnetoencephalography towards real-world applications with a wearable system. *Nature*. 2018; 555: 657–661.
4. Savukov IM, Romalis MV. Nmr detection with an atomic magnetometer. *Physical Review Letters*. 2005; 94: 123001.
5. Hämäläinen M, Hari R, Riitta. Magnetoencephalographic characterization of dynamic brain activation: Basic principles and methods of data collection and source analysis. In: AW Toga, JC Mazziotta, editors. *Brain mapping: The methods*. New York: Elsevier Science. 2002; 227–253.
6. Hämäläinen M, Hari R, Ilmoniemi RJ, Knuutila J, Lounasmaa OV. Magnetoencephalography - theory, instrumentation, and applications to noninvasive studies of the working human brain. *Reviews of Modern Physics*. 1993; 65: 413–497.
7. Singh KD. Magnetoencephalography. In: C Senior, T Russell, M Gazzaniga, editors. *Methods in mind*. Cambridge: MIT Press. 2006; 291–326.
8. Peters A, Jones EG. *Cerebral cortex*. Vol. 1. Cellular components of the cerebral cortex. New York: Plenum. 1984.
9. Koch C. *Biophysics of computation: Information processing in single neurons*. Oxford, UK: Oxford University Press. 1999.

10. Da Silva FHL. Electrophysiological basis of MEG signals. In: PC Hansen, ML Kringelbach, R Salmelin, editors. MEG: An introduction to methods. Oxford: Oxford University Press. 2010; 1–23.
11. Vrba J, Robinson SE. Signal processing in Magnetoencephalography. *Methods*. 2001; 25: 249–271.
12. Bardeen J, Cooper LN, Schrieffer JR. Theory of superconductivity. *Physical Review*. 1957; 108: 1175–1204.
13. Josephson BD. Possible new effects in superconductive tunneling. *Physics Letters*. 1952; 1: 251–253.
14. Clarke J. SQUIDs. *Scientific American*. 1994; 271: 46–53.
15. Clarke J. SQUID fundamentals. In: H Weinstock, editor. SQUID sensors: Fundamentals, fabrication and applications. Berlin: Springer. 1996; 1–62.
16. Forgacs RL. Digital-analog magnetometer utilizing superconducting sensor. *Review of Scientific Instruments*. 1967; 38: 214.
17. Clarke J. SQUIDs: Theory and practice. In: H Weinstock, RW Ralston, editors. The new superconducting electronics. Netherlands: Kluwer Academic Publisher. 1993; 123–180.
18. Braginski AI, Krause HJ, Vrba J. SQUID Magnetometers. In: MH Francombe, editor. Handbook of thin film devices. 2000; 3: 149–225.
19. Drung D, Mück M. SQUID electronics. In: J Clarke, AI Braginski, editors. The SQUID handbook: Vol.I Fundamentals and technology of SQUIDs and SQUID Systems. Weinheim: Wiley-Vch Verlag GmbH & Co. 2004; 127–170.
20. Ketchen MB, Bhushan M, Kaplan SB, Gallagher WJ. Low noise DC SQUIDs fabricated in Nb-Al<sub>2</sub>O<sub>3</sub>-Nb trilayer technology. *IEEE Transactions on Magnetics*. 1991; 27: 3005–3008.

21. Cantor R, Ludwig F. SQUID Fabrication Technology. In: J Clarke, AI Braginski, editors. The SQUID handbook: Vol. I Fundamentals and technology of SQUIDs and SQUID Systems. Weinheim: Wiley-Vch Verlag GmbH & Co. 2004; 93–125.
22. Cantor R, Koelle, D. Practical DC SQUIDS: Configuration and performance. In: J Clarke, AI Braginski, editors. The SQUID handbook: Vol. I Fundamentals and technology of SQUIDs and SQUID Systems. Weinheim: Wiley-Vch Verlag GmbH & Co. 2004; 171–217.
23. Parkkonen L. Instrumentation and data preprocessing. In: PC Hansen, ML Kringelbach, R Salmelin, editors. MEG: An introduction to methods. Oxford: Oxford University Press. 2010; 24–64.
24. Bork J, Hahlbohm HD, Klein R, Schnabel A. The 8-layered magnetically shielded room of the ptb: Design and construction. In: J Nenonen, RJ Ilmoniemi, T Katila, editors. Biomag 2000, Proceedings of the 12th international conference on biomagnetism. Helsinki University of Technology, Espoo, Finland 2000. 2000; 970–973.
25. Vacuumschmelze GmbH & Co. Operating instructions: Shielding cabin. 2014. Retrieved from <http://www.vacuumschmelze.com>
26. Elekta Neuromag Triux. Elekta Neuromag Triux: State-of-the-art Magnetoencephalography. 1998. Web Page. Retrieved from <https://www.elekta.com/meg>
27. CTF MEG system. CTF MEG: The technology leader in MEG instrumentation. 1970. Web Page. Retrieved from <http://www.ctfmeg.com>
28. Kado H, Higuchi M, Shimogawara M, Haruta Y, Adachi Y, et al. Magnetoencephalogram Systems developed at KIT.

- IEEE Transactionson Applied Superconductivity. 1990; 9: 4057–4062.
29. Adachi Y, Miyamoto M, Kawai J, Kawabata M, Higuchi M, et al. Development of a whole-head child meg system. In: S Supek, A Sušac, editors. *Advances in Biomagnetism*. Berlin: Springer. 2010; 28: 35–38.
  30. Johnson BW, Crain S, Thornton R, Tesan G, Reid M. Measurement of brain function in pre-school children using a custom sized whole-head MEG sensor array. *Clinical Neurophysiology*. 2010; 121: 340–349.
  31. Okada Y, Pratt K, Atwood C, Mascarenas A, Reineman R, et al. BabySQUID: A mobile, high-resolution multichannel magnetoencephalography system for neonatal brain assessment. *Review of Scientific Instruments*. 2006; 77: 024301.
  32. Roberts TP, Paulson DN, Hirschhoff E, Pratt K, Mascarenas A, et al. Artemis 123: Development of a whole-head infant and young child MEG system. *Frontiers in Human Neuroscience*. 2014; 8: 99.
  33. Robinson SE, Burbank MB, Fife AA, Haid G, Kubik PR, et al. A biomagnetic instrument for human reproductive assessment. In: J Nenonen, RJ Ilmoniemi, T Katila, T korkeakoulu, Lt laboratorio, editors. *Biomag 2000: Proceedings of the 12th International Conference on Biomagnetism*. Espoo, Finland: Helsinki University of Technology. 2000.
  34. Vrba J, Nenonen J, Trahms L. Biomagnetism. In: J Clarke, AI Braginski, editors. *The SQUID handbook: Vol. II Applications of SQUIDS and SQUIDS systems*. Weinheim: Wiley-Vch. 2006; 389.
  35. Johnsrude IS, Hauk O. Neuroimaging: Techniques for examining human brain function. In: N Braisby, editor. *Cognitive psychology: A methods companion*. Oxford: Oxford University Press. 2005.

36. Min BK, Marzelli MJ, Yoo SS. Neuroimaging-based approaches in the brain-computer interface. *Trends in Biotechnology*. 2010; 28: 552–560.
37. Nicolas-Alonso LF, Gomez-Gil J. Brain computer interfaces, a review. *Sensors*. 2012; 12: 1211–1279.
38. Baillet S. Magnetoencephalography for brain electrophysiology and imaging. *Nature Neuroscience*. 2012; 20: 327–339.
39. Tan HR, Gross J, Uhlhaas PJ. Meg-measured auditory steady-state oscillations show high test-retest reliability: A sensor and source-space analysis. *Neuroimage*. 2015; 122: 417–426.
40. Cottureau B, Lorenceau J, Gramfort A, Clerc M, Thirion B, et al. Phase delays within visual cortex shape the response to steady-state visual stimulation. *Neuroimage*. 2011; 54: 1919–1929.
41. Koelewijn L, Rich AN, Muthukumaraswamy SD, Singh KD. Spatial attention increases high-frequency gamma synchronisation in human medial visual cortex. *Neuroimage*. 2013; 79: 295–303.
42. Jerbi K, Lachaux JP, N'Diaye K, Pantazis D, Leahy RM, et al. Coherent neural representation of hand speed in humans revealed by meg imaging. *Proceedings of the National Academy of Sciences of the United States of America*. 2007; 104: 7676–7681.
43. Baldauf D, Desimone R. Neural mechanisms of object-based attention. *Science*. 2014; 344: 424–427.
44. Landau AN, Schreyer HM, van Pelt S, Fries P. Distributed attention is implemented through theta-rhythmic gamma modulation. *Current Biology*. 2015; 25: 2332–2337.

45. Tallon-Baudry C. On the neural mechanisms subserving consciousness and attention. *Frontiers in Psychology*. 2011; 2: 397.
46. Bourguignon M, De Tieghe X, de Beeck MO, Ligot N, Paquier P, et al. The pace of prosodic phrasing couples the listener's cortex to the reader's voice. *Human Brain Mapping*. 2013; 34: 314–326.
47. Ding N, Melloni L, Zhang H, Tian X, Poeppel D. Cortical track-ing of hierarchical linguistic structures in connected speech. *Nature Neuro-science*. 2016; 19: 158–164.
48. Doelling KB, Poeppel D. Cortical entrainment to music and its modulation by expertise. *Proceedings of the National Academy of Sciences of the United States of America*. 2015; 112: E6233–E6242.
49. Zhao TC, Kuhl PK. Musical intervention enhances infants' neu-ral processing of temporal structure in music and speech. *Proceedings of the National Academy of Sciences*. 2016; 113: 5212–5217.
50. Anderson CT, Carlson CE, Li Z, Raghavan M. Magnetoen-cephalography in the preoperative evaluation for epilepsy surgery. *Current Neurology and Neuroscience Reports*. 2014; 14: 446.
51. Kharkar S, Knowlton R. Magnetoencephalography in the presurgical evaluation of epilepsy. *Epilepsy & Behavior*. 2015; 46: 19–26.
52. Murakami H, Wang ZI, Marashly A, Krishnan B, Prayson RA, et al. Correlating magnetoencephalography to stereo-electroencephalography in patients undergoing epilepsy surgery. *Brain*. 2016; 139: 2935–2947.
53. Rose D, Smith P, Sato S. Magnetoencephalography and epi-lespy research. *Science*. 1987; 238: 329–335.

54. Port RG, Anwar AR, Ku M, Carlson GC, Siegel SJ, et al. Prospective meg biomarkers in asd: Pre-clinical evidence and clinical promise of electrophysiological signatures. *The Yale Journal of Biology and Medicine*. 2015; 88: 25–36.
55. Roberts TP, Khan SY, Rey M, Monroe JF, Cannon K, et al. Meg detection of delayed auditory evoked responses in autism spectrum disorders: Towards an imaging biomarker for autism. *Autism Research*. 2010; 3: 8–18.
56. Schnitzler A, Timmermann L, Gross J. Physiological and pathological oscillatory networks in the human motor system. *Journal of Physiology – Paris*. 2006; 99: 3–7.
57. Hansen PC, Kringelbach ML, Salmelin R. *Meg: An introduction to methods*. Oxford: Oxford University Press. 2010.
58. Hari R, Salmelin R. *Magnetoencephalography: From squids to neuroscience*. *Neuroimage*. 2012; 61: 386–396.
59. Supek S, Aine CJ. *Magnetoencephalography: From signals to dynamic cortical networks*. New York: Springer. 2014.
60. Vrba J. *Magnetoencephalography: The art of finding a needle in a haystack*. *Physica C*. 2002; 368: 1–9.